Turkish Journal of Earth Sciences

Volume 34 | Number 7 Article 3

11-25-2025

Deformation conditions and quantifying strain in the Chai-Kour shear zone in the Zagros orogenic belt of Iran

SAEEDE KESHAVARZ

SAEED ZAREI

MAJID SHAHPASANDZADEH

SOUMYAJIT MUKHERJEE

Recommended Citation
KESHAVARZ, S, ZAREI, S, SHAHPASANDZADEH, M, & MUKHERJEE, S (2025). Deformation conditions and quantifying strain in the Chai-Kour shear zone in the Zagros orogenic belt of Iran. *Turkish Journal of Earth Sciences 34* (7): 824-844. https://doi.org/10.55730/1300-0985.1996

TÜBİTAK

Turkish Journal of Earth Sciences

http://journals.tubitak.gov.tr/earth/

Research Article

Turkish J Earth Sci
(2025) 34: 824-844

doi:10.55730/1300-0985.1996

Deformation conditions and quantifying strain in the Chai-Kour shear zone in the Zagros orogenic belt of Iran

Saeede KESHAVARZ[1,2,*], Saeed ZAREI[2], Majid SHAHPASANDZADEH[1], Soumyajit MUKHERJEE[3]

[1]Department of Earth Sciences, Graduate University of Advanced Technology, Kerman, Iran
[2]Department of Geophysics, Faculty of Nano and Bio Science and Technology, Persian Gulf University, Bushehr, Iran
[3]Department of Earth Sciences, Indian Institute of Technology Bombay, Powai, Mumbai, Maharashtra, India

Received: 08.10.2024 • **Accepted/Published Online:** 15.10.2025 • **Final Version:** 25.11.2025

Abstract: Strain analyses and kinematic studies in orogenic belts are essential for understanding their deformation mechanisms. The Chai-Kour brittle-ductile shear zone is located in the central Sanandaj-Sirjan metamorphic belt, southeast of the Zagros orogen. The present study analyzes deformed mylonitic rocks to clarify the deformation kinematics, temperature, and strain geometry of the Chai-Kour shear zone. Previously developed kinematic shear indicators such as S-C shear bands, deformed porphyroclasts, asymmetric boudins, and folds provide an overall top-to-the-southeast sense of shear in the Chai-Kour shear zone. Quartz micro-thermometry confirms that the Chai-Kour rocks were initially affected by a high-temperature (550–650 °C) deformation that was followed by a post-superimposed low-temperature (380–420 °C) deformation. Rf/ϕ strain measurements reveal a plane-strain deformation geometry. The estimated W_m by the Rigid Grain Net technique ranges from 0.54 to 0.73, suggesting simultaneous contributions of simple (38–54%) and pure (46–62%) shear components. Spatial variation of deformation indicates that the simple shear component increases towards the northeast and southwest boundaries of the shear zone. The present study suggests that this shear zone experienced a 55–75% shortening perpendicular to its boundaries. These deformation characteristics in the Chai-Kour shear zone have been influenced primarily by a transpressive tectonic regime with lateral extrusion, resulting from the continuing oblique convergence of the Afro-Arabian plate with the continental crust of central Iran. This tectonic evolution resembles that experienced in other collisional zones, such as the Alpine and Himalayan orogens.

Key words: Microstructures, ductile shearing, deformation temperature, strain portioning, Zagros, Chai-Kour shear zone

1. Introduction

In continent-continent collision systems, major crustal deformations occur due to the accumulated strain in the midcrustal shear zones that develop at different scales, from microscopic shear bands to multi-km deformation zones (Xypolias et al., 2010; Mookerjee et al., 2016; Sarkarinejad et al., 2017; Mukherjee, 2019). To understand the flow conditions in these zones, quantitative kinematic analyses of shear zones are essential (e.g., Mukherjee, 2010). There have been numerous studies to date analyzing the tectonics and kinematics of ductile shear zones, combining quantified analyses of strain with measurements of kinematic vorticity in mylonitic rocks (Mukherjee and Biswas, 2014; Roy et al., 2016; Bose and Mukherjee, 2020; Derikvand and Almasi, 2022; Mansouri et al., 2023). Strain partitioning in shear zones is quantified based on the kinematic vorticity number (W_k)—a useful parameter for the reconstruction of deformation history (Bose et al., 2019; Mohammad et al., 2020; Meher et al., 2020), and the development of extrusion models for a shear zone (Mukherjee and Koyi, 2010; Law et al., 2010; Mukherjee, 2013; Tiwari et al., 2020; Ahanger and Jeelani, 2022). Xypolias (2010) carried out a study of the different vorticity analysis methods applied to the study of shear zones in various tectonic settings, highlighting also their limitations.

In natural shear zones, strain is generally spatially nonuniform, and includes both coaxial (Mukherjee, 2012, 2019) and noncoaxial components in subsimple deformations (Frassi et al., 2009; Sarkarinejad et al., 2015; Keshavarz and Faghih, 2020; Simonetti et al., 2020a; Mansouri et al., 2021). Ramberg (1975) proposed a three-dimensional model for application to general or subsimple shear zones, especially in the context of transpression and transtension (e.g., Sanderson and Marchini, 1984; Simpson and De Paor, 1993; Tikoff and Fossen, 1993). Díaz-Azpiroz et al. (2016) described a standard approach to kinematic analysis, contributing to a better understanding

* Correspondence: saeede388@gmail.com, s.keshavarz@kgut.ac.ir

of deformation in shear zones. The heterogeneity of the constitutive properties of natural transpressive (or transtensional) zones affects both their structural style and deformation mechanics. Three-dimensional finite element models incorporating an elasto-plastic rheology have been used to investigate the structural and mechanical evolution of transpression zones (Nabavi et al., 2018, 2020). Recent studies have provided valuable structural data on the regional implications of transpersion/transtension zones, making use of multidisciplinary approaches to estimate temperature, absolute timing, and deformation conditions (such as strain geometry and kinematics of flow) (Simonetti et al., 2020a; Dias et al., 2022; Montemagni and Zanchetta, 2022; Petroccia et al., 2022; Petroccia et al., 2024). Studies of three-dimensional strain patterns involve the identification of various geometries of strain ellipsoids and strain tensors (Flinn, 1962, 1978; Jiang and Williams, 1998; Passchier, 1998). Investigations of three-dimensional kinematic vorticity reveal deformation settings to be highly complex, and differ significantly from those identified through two-dimensional approaches (Carreras et al., 2013).

The Iranian section of the Alpine-Himalayan mountain range was formed by the continental convergence of the Arabian and Eurasian cratons since the Late Paleozoic era (Madanipour et al., 2024). Multiple subsequent deformation events occurred during the tectonic evolution of the Iranian mountain-building associated with the Gondwana rifting and the Arabian plate collision. These events resulted in the formation of the Alborz to Kopeh-Dagh range, central Iranian block, Lut block, East Iranian belt, Zagros orogen, and Makran subduction zone (Zonenshain and Pichon, 1986; Allen et al., 2004; Sadeghi et al., 2023, Figure 1a). There have been several field-based and theoretical studies of the geological and structural outcomes of the oblique collisions in the Zagros orogeny (Mohajjel and Fergusson, 2000; Fergusson et al., 2016; Behyari and Shahbazi, 2019; Sheikholeslami et al., 2019; Keshavarz and Faghih, 2020; Partabian and Faghih, 2021; Mansouri et al., 2023; Madanipour et al., 2024).

The principal objective of this research is to investigate the flow kinematics and predominant strain pattern associated with the deformation along the Chai-Kour shear zone based on the results of field observations, structural characteristic analyses, and strain measurements. The study further evaluates whether these deformations correspond to those along the Sanandaj-Sirjan metamorphic belt in southeastern Iran, for which the finite strain and vorticity number (W_k) of the flow regime along the northeast-southwest transect across the shear zone are calculated. These quantified results in the Chai-Kour shear zone not only elucidate the local deformation mechanisms but also provide insights into the larger-scale crustal dynamics of the Zagros orogen, particularly how strain partitioning accommodates oblique plate convergence.

2. Geological setting

The Zagros Mountains form a shortened and thickened collisional orogen located in the central segment of the Alpine-Himalayan mountain range. Detailed studies documenting the structure and deformation characteristics of such orogenic belts contribute to the understanding of the processes of global orogeny. This belt extends 1200 km from the Anatolian fault system (SE, Türkiye) to the Minab–Zendan fault system (S, Iran). A series of long-standing and complex tectonic events from Late Cretaceous to Early Tertiary led to the emergence of the Zagros orogen, including: (i) the opening of the Neo-Tethyan Ocean between the Eurasian and Arabian Plates, (ii) the northward subduction/obduction of the Neo-Tethyan oceanic crust following the convergence of the Arabian plate, and (iii) the collision of the Arabian and Eurasian plates (Mohajjel and Fergussen, 2000; Alavi, 2004; Madanipour et al., 2024). A study by Vernant et al. (2004) using GPS data reveals that the motion of Arabian plate is continuing approximately 20 ± 2 mm yr^{1} toward N11° ± 5° E.

This orogenic belt is subdivided in a northeast to southwest direction into the northwest-trending parallel tectono-metamorphic and magmatic belts (Figure 1a, Alavi, 2004; Agard et al., 2005; Agard et al., 2011; Mouthereau et al., 2012). (1) The Urumieh-Dokhtar magmatic arc is a linear magmatic zone that has been active since the Late Cretaceous to the Eocene (Alavi, 2004).

(2) The Sanandaj-Sirjan metamorphic belt (nearly 1500 km long and 150–200 km wide), lying alongside the southern edge of the Eurasian plate, is composed of Paleozoic to Cretaceous sedimentary and metamorphic rocks in the former active margin of the Iranian microcontinent that drifted during the Late Jurassic, and ultimately collided with the Arabian margin during the Miocene (Mouthereau et al., 2012). The metamorphic rocks in this belt are classified into two HP/LT and LP/HT belts, which formed during transpressional deformation associated with the Neo-Tethyian subduction (Sarkarinejad and Azizi, 2008). The $^{40}Ar/^{39}Ar$ dating of biotite gneiss from the Neyriz area yields ages of 119.95 ± 0.88 Ma and 112.58 ± 0.66 Ma (Sarkarinejad et al., 2009). The Phanerozoic (non)metamorphosed rocks in this belt moved and were imbricated toward the passive margin of the Afro-Arabian plate through the activity of thrust systems, occurring along a northeast-southwest trend from the suture zone toward the interior of the Arabian craton (Alavi, 2004). This belt features widespread structures such as imbricate thrust zones, thrust-related folds, duplex structures, brittle to ductile shear zones, and penetrative foliations and lineations (Sarkarinejad et al., 2007).

(3) The Zagros Fold-and-Thrust Belt comprises 12–13 km of sedimentary rock cover from Cambrian up to the

Recent, lying in the external part of the orogen belt (Agard et al., 2011). The belt is divided into the Simply Folded Belt and the Imbricate Zone, and is separated from the Sanandaj-Sirjan metamorphic belt by the Main Zagros thrust fault or suture zone (Vergés et al., 2024).

The Chai-Kour shear zone, measuring 26 km in length and varying in width from 3 km to 15 km**,** occupies the SE part of Sanandaj-Sirjan metamorphic belt, located in the Baghat region**,** approximately 100 km south of Sirjan in southeast Iran (Figure 1a). This shear zone is bounded by northwest to southeast-striking thrust faults, dipping to the northeast. This area provides an excellent opportunity to study the structural characteristics of sheared rocks within the midcrustal deformed zone of the Zagros collisional regime, containing highly deformed Paleozoic–Mesozoic metamorphic outcrops of sandstone, greenschist, mica schist, augen gneiss, amphibolite, marble, and dolo-marble (Figure 1b). These metamorphic units have undergone mylonitization, and penetrative deformation structures are well developed.

3. Structural architecture

Exposed outcrops with well-developed brittle and ductile structures at various scales were selected for detailed analysis. Accordingly, 11 oriented samples were collected from along the northeast-southwest section and their deformed microstructures, strain geometries, and W_k numbers were evaluated (Figure 1c).

3.1. Mesostructures

The metamorphic rocks in the Chai-Kour shear zone hold records of polyphase deformations. The early deformation phase (D_1) produced a well-developed foliation (S_1) in mica-schists and phyllites**,** formed out of layered silicates/flattened/stretched grains. This foliation wraps around porphyroclasts and asymmetric boudins in mylonites. The S_1 Foliation strikes west–east and dips 15°–40° toward the north-northeast (Figure 1c). This foliation is thought to have been considerably modified by the D_2 deformation, during which asymmetric crenulation cleavage and microfolds developed (Mukherjee et al., 2015) in the Chai-Kour Shear Zone (Figure 2a). We concluded from field observations and equal-area stereonet projections that S_2 is oriented at a 30°–40° angle with respect to the S_1 foliation.

Our observations also revealed two generations of lineations. The first group of lineations (L_1) is defined by the preferred alignment of stretched quartz and feldspar, trending from N50°E to N75°E, with plunges ranging from 9° to 30°. The Second generation of lineations (L_2) is defined by the intersections of S_1 and S_2 in microfolds or crenulation cleavage (Fossen, 2016; Passchier and Trouw, 2005), with subhorizontal plunges toward the southeast.

Well-exposed (proto)mylonites characterize the northwest–southeast trending Chai-Kour Shear Zone (Figure 2b). Penetrative asymmetic porphyroclasts (σ and δ-type) and S–C fabrics can be seen in the studied sample (Figures 2c–2e), primarily K-feldspar, with fine-grained tails drawn out subparallel to the direction of the C-plane. Ductile shearing in the deformed outcrops produced asymmetric shear band boudins (Figure 2f, Mukherjee, 2017; Goscombe et al., 2004;), Z-type folds, and box folds (Figures 2g and 2h, Twiss and Moores, 2006; Nabavi and Fossen, 2021).

3.2. Microstructures

At the microscale, major microstructures can be seen in the deformed coarse- and fine-grained samples. Microstructural analyses were conducted on thin sections cut parallel to the lineation and perpendicular to the foliation (XZ-planes). Elongated ribbon quartz can be identified within the foliation plane (Figure 3a). Both disjunctive (Figure 3a) and coarse continuous foliation can be observed in the mica schists, based on the classification developed by Twiss and Moores (2006). Quartz ribbons, mica fish, and rotated grains with asymmetric tails are apparent (Figures 3a–3d). Some 35–45% of the deformed clasts are quartz and feldspar grains, while 50–55% of the fine-grained matrix consisting of such minerals as mica, quartz, and amphibole.

Sigma and delta-type K-feldspar porphyroclasts are predominant in the (proto)mylonites. The long axes of porphyroclasts are oriented subparallel to the S-plane, and the tails follow the C-plane (Figures 3b and 3c). Muscovite fish display cleavages that are locally oriented subparallel to the S foliation (Figure 3b, e.g., Mukherjee, 2011). Additionally, fractured feldspars exhibiting slip along the synthetic micro fault plane and backward or forward rotations of broken fragments have formed "bookshelf" structures (Mukherjee and Khonsari, 2018; Figure 3d).

4. Methodology

4.1. Quartz microthermometry

Different deformation mechanisms are typically associated with specific temperature ranges (Stipp et al., 2002a; Passchier and Trouw, 2005; reviewed in Bose and Mukherjee, 2020). Quartz in particular displays various deformation behaviors under different temperature conditions. Quartz dynamic recrystallization regimes are widely used as a deformation thermometer during mylonitization (Jessell and Lister, 1990; Stipp et al., 2002b; Tullis, 2002). Dynamic recrystallization is influenced by strain rate, temperature, and hydrolytic weakening (Law, 2014). Bulging recrystallization (BLG) corresponds to regime 1, and is dominant during low temperature deformations (280–400 °C). Subgrain rotation recrystallization (SGR) microstructures (400–500 °C, dislocation creep regime 2) become dominant as temperatures increase or as the strain rate decreases. In such cases, a rapid dislocation climb rate can be expected. At

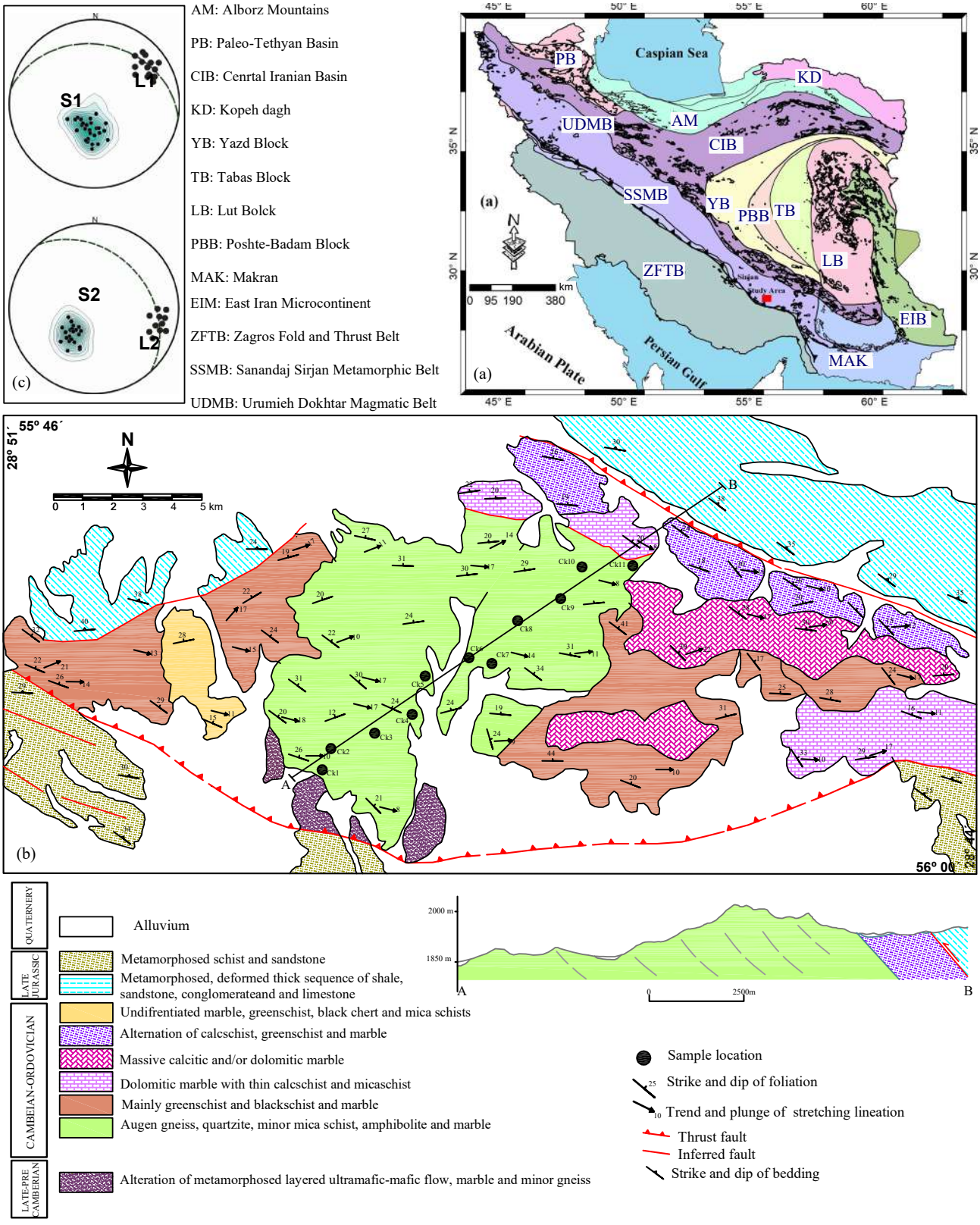

Figure 1. (a) Inset map: tectonic units forming the Iranian plateau (modified from Aghanabati, 2004). Red rectangle: location of the Chai-Kour shear zone; (b) Detailed geology map of the study area (Modified after Sabzehei, 1996). The sampling locations for the strain analysis; (c) Stereo-plot of foliations and lineations.

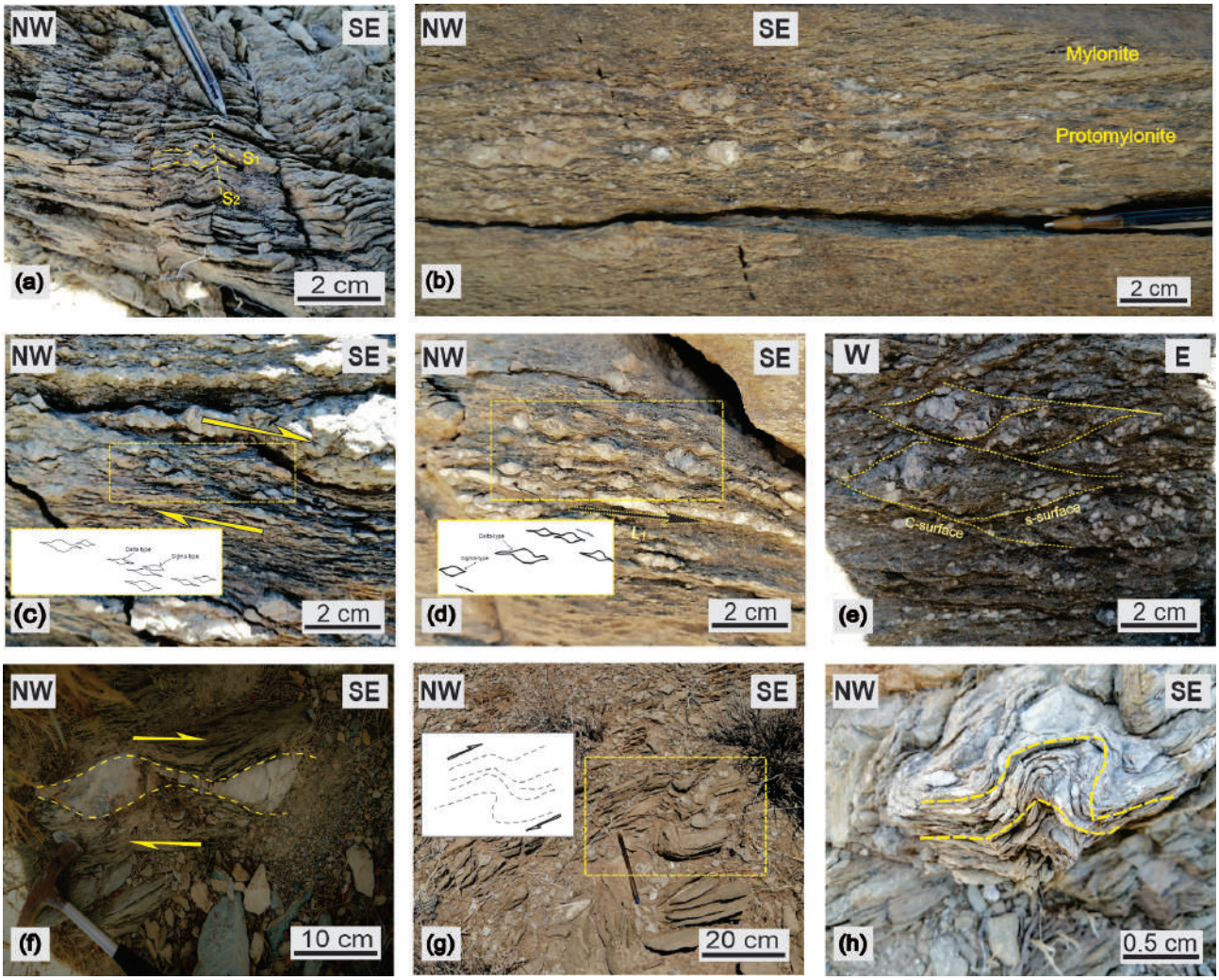

Figure 2. Field photographs of deformed rocks on XZ planes in the Chai-Kour shear zone. (a) S1 and S2 foliations. Alternating S1 foliations with small-scale tight folds with axial surfaces parallel to S2 foliations. (b) Outcrop-scale of (proto)mylonites. (c), (d) σ and δ-type rotated porphyroclats. (e) S-C shear structures. (f) Asymmetric shear band boudin. (g) Z-type fold. (h) Box fold.

higher temperatures (>500 °C), grain-boundary migration (GBM) recrystallization microstructures dominate, with subgrain nucleation occurring as a result of rapid, diffusion-controlled dislocation climb (dislocation creep regime 3). A transition from subgrain rotation to grain-boundary migration can occur when a local decrease in strain rate occurs (Tullis, 2002; Stipp et al., 2010). The dynamic recrystallization analyses of quartz in the selected samples reveal a dominance of GBM recrystallization in the grains, accompanied by SGR mechanisms (Figure 3a), with only minor microstructural evidence of bulging grain boundaries (BLG; Figures 3e,3f).

4.2. Finite strain analysis

For the finite strain analysis of the deformed samples, we used the Microsoft Excel spreadsheet developed by Chew (2003) for the R_f/φ technique (Ramsay, 1967; Dunnet, 1969; Lisle, 1985). Several key factors must be considered for an accurate strain analysis. For example, fractured porphyroclasts and recrystallized grains should be excluded from the strain measurement (Figures 4a–4c), whereas plastically elongated porphyroclasts should behave as freely-rotating rigid ellipsoids and should not mechanically interact with one another (Figure 4d, Bose et al., 2018).

Three thin sections were prepared from each specimen: (1) YZ plane (normal to both the lineation and foliation), (2) XZ plane (parallel to the lineation and normal to the foliation), and (3) XY plane (parallel to the foliation). The Φ angle and aspect ratio (R_f = long axis/short axis) of each porphyroclast were then measured, Φ being the angle between the long axes of the porphyroclasts and the trace of mylonitic foliation. Approximately 80 isolated

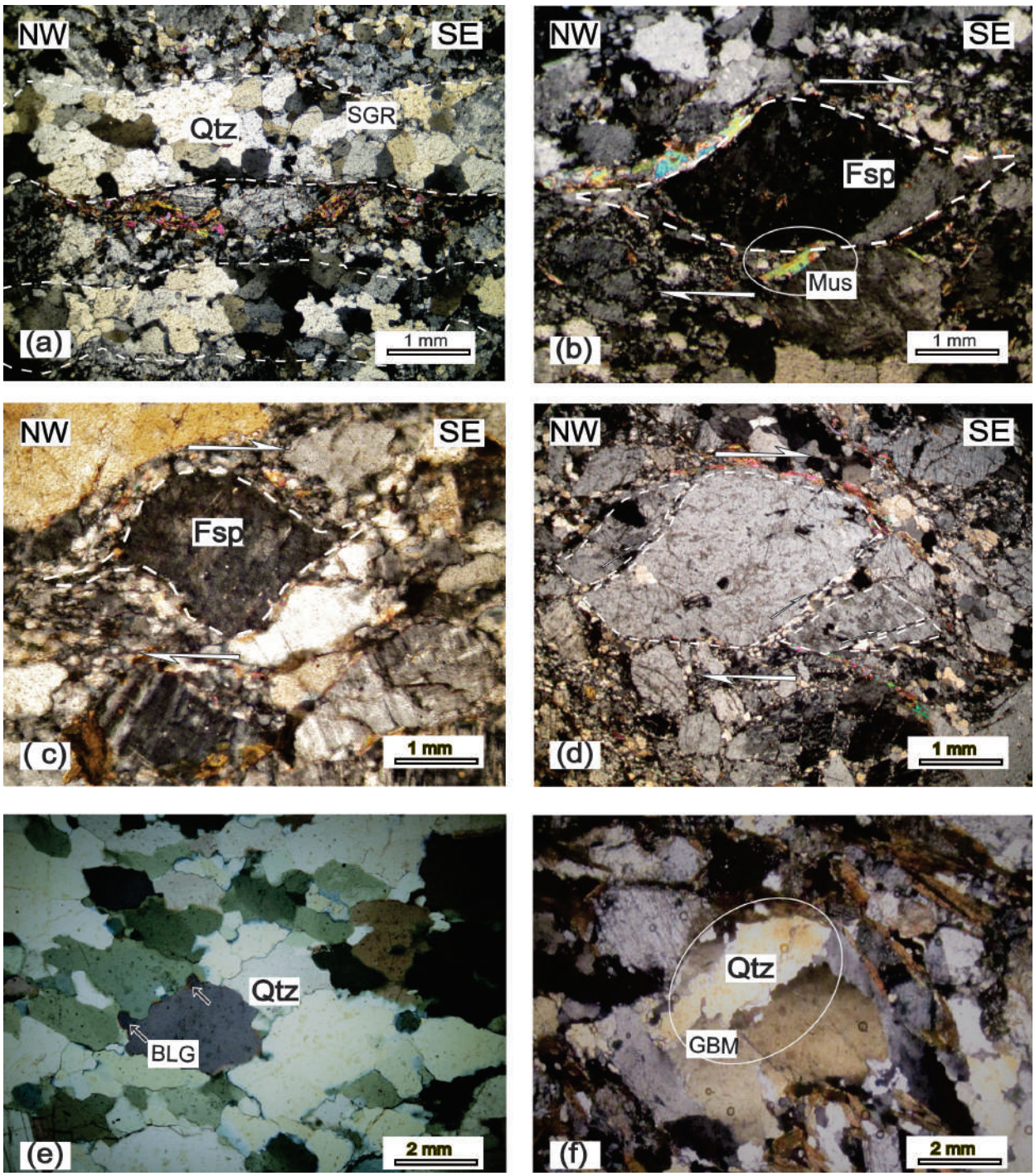

Figure 3. Photomicrograph of microstructures in quartzo-feldspathic rocks. (a) Quartz ribbon with subgrain rotation recrystallization (SGR). (b) σ-type porphyroclasts enclosed in a fine grain matrix composed of recrystallized quartz and mica. (c) δ-type porphyroclasts of feldspar embedded in a matrix of fine grain quartz with subgrain migration recrystallization. (d) Slip along cleavages of feldspar porphyroclast, under top-to-SE shearing formed "bookshelf" structure. (e) Bulging recrystallization in quartz grain boundary (BLG). (f) Quartz grain boundary migration recrystallization (GBM).

porphyroclasts were measured in each thin section (Faghih and Soleimani, 2015), yielding R_s values (Rs = axial ratio of the strain ellipse) and Rf/Φ graphs. Symmetry and θ-distribution tests (χ^2) were conducted to assess the initial random orientation of grains and to determine the best-fitting curve for Rs, respectively. The shape and geometry

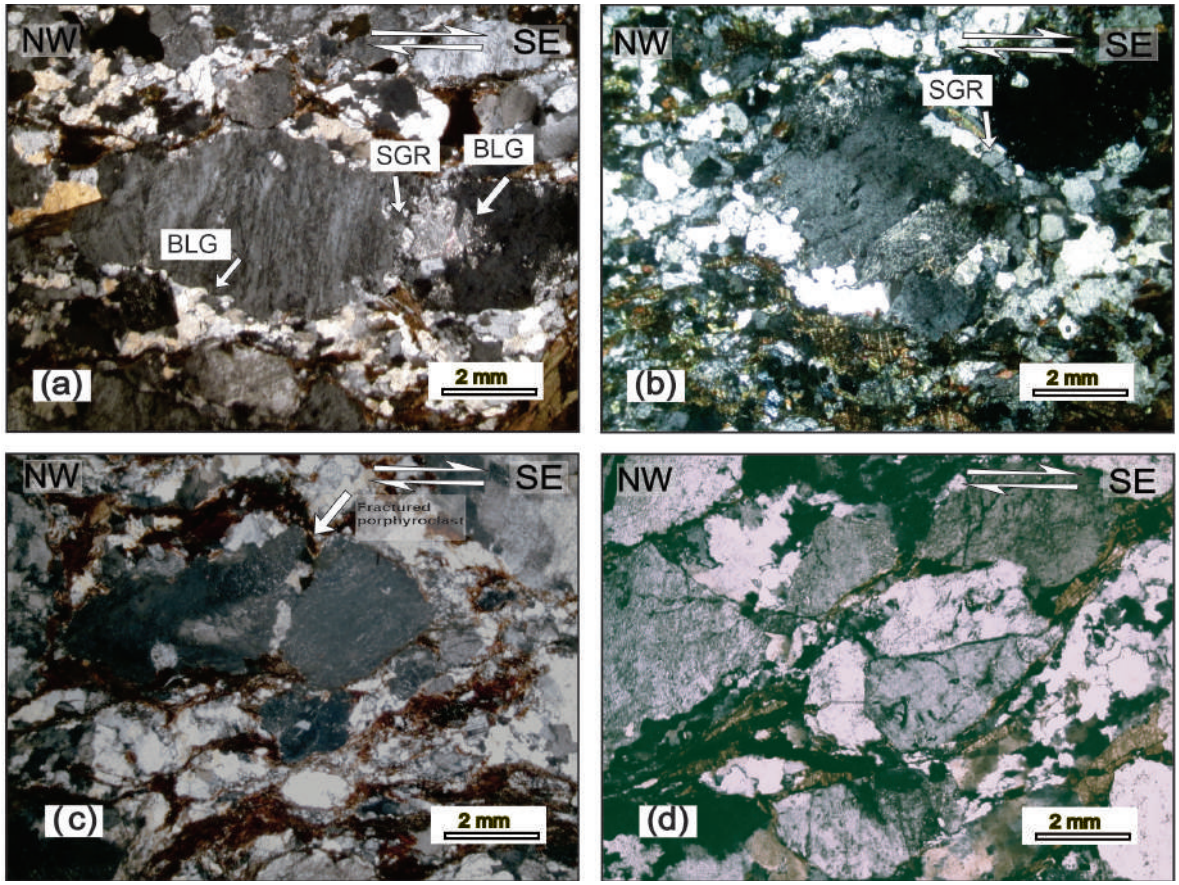

Figure 4. Grains avoided in strain measurement (a and b) recrystallized feldspar. (c) Fractured porphyroclasts. (d) Grain with mechanical interactions.

of the strain ellipsoid on the Flinn diagram were analyzed using the Strain & Shear Calculator 3.2 program[1]. Flinn's K-value and natural logarithmic strain(ε) are defined as:

$$K=R_{XZ}\text{-}1/R_{YZ}\text{-}1 \quad \text{(eq. 1)}$$

$$\varepsilon=(1/\sqrt{3})(\sqrt{(\varepsilon_1-\varepsilon_1)^2+(\varepsilon_2-\varepsilon_3)^2+(\varepsilon_3-\varepsilon_1)^2}) \quad \text{(eq. 2)}$$

where $\varepsilon_{1,2,3}$ are the natural strains of the long, intermediate, and short principal axis lengths of the strain ellipsoid, respectively. The results of the strain analysis are presented in Table 1 and Figure 5.

4.3. Kinematic vorticity number (W_k)

In natural shear zones, noncoaxial flow is typically characterized using the kinematic vorticity number (W_k), calculated using the formula $W_k = \cos(\alpha)$, where α is the angle estimated between the two flow apophyses (Passchier, 1987; Fossen, 2016). This dimensionless parameter is classified on a nonlinear scale and represents the relative contributions of coaxial and noncoaxial deformation: (1) subsimple shear deformation, $0 < W_k < 1$; (2) coaxial deformation with α =90° and $W_k = 0$; and (3) noncoaxial (simple shear) deformation with α =0° and $W_k = 1$. Among the various methods and assumptions developed over time to measure W_k, this research utilizes the rigid clast rotation-based method. In a pioneering analytical study, Jeffery (1922) proposed that the rotation of rigid grains in a deforming matrix can constrain the relative contributions of pure and simple shear. Subsequent studies have extended these principles from theoretical models to natural deformed samples (Xypolias, 2010 and references therein). Clast-based vorticity gauges are now widely used to reveal the deformation kinematics in natural shear zones in various tectonic settings (Xypolias, 2007). These analyses are based on mathematical relationships between the vorticity number (W_m), the aspect ratio of porphyroclasts (R), and the Φ angle (the angle between long axis of a porphyroclast and the foliation (Simpson and De Paor, 1993, 1997)). As an advanced approach, the Rigid Grain Net (RGN) plots the *R* parameter and Φ in the

[1] Rod Holcombe Software Home Page[online]. Website https://www.holcombe.net.au http://opensees.berkeley.edu/OpenSees/home/about.php [accessed 12 December 2024].

Table 1. Flinn's *K*-value and Lode's ratio (Lode 1926; Flinn 1962) – general parameters that show the geometry and shape of strain ellipsoids.

Sample	R_{xy}	R_{yz}	R_{xz}	X: Y: Z	k	£s	Lode's parameter
Ck1	2.10	2.00	4.20	2.07:0.98:0.49	1.10	1.010	0.034
Ck2	1.90	1.95	3.71	1.92:1.01:0.52	0.95	0.926	0.020
Ck3	1.60	1.73	2.77	1.64:1.03:0.59	0.82	0.720	0.077
Ck4	1.65	1.75	2.89	1.68:1.02:0.58	0.87	0.750	0.055
Ck5	1.50	1.49	2.24	1.50:1.0:00.67	1.02	0.570	0.008
Ck6	1.50	1.55	2.33	1.52:1.01:0.65	0.91	0.590	0.039
Ck7	1.75	1.90	3.33	1.08:1.03:0.54	0.83	0.850	0.068
Ck8	1.68	1.60	2.69	1.65:0.98:0.61	1.13	0.690	0.049
Ck9	2.00	2.10	4.20	2.03:1.02:0.48	0.91	1.010	0.034
Ck10	1.80	2.30	4.14	1.95:1.09:0.47	0.72	1.010	0.173
Ck11	2.10	2.15	4.52	2.12:1.01:0.47	0.96	1.070	0.016

Note: All parameters are unitless.

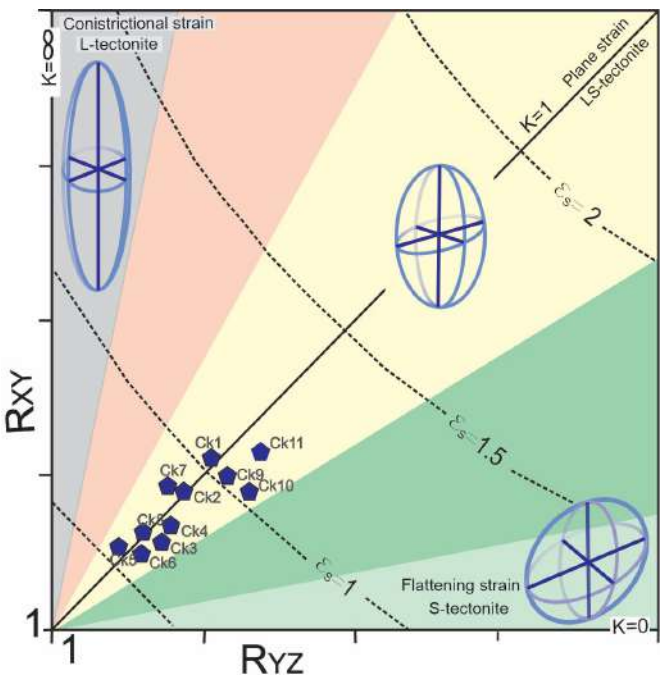

Figure 5. Finite strain data from the Chai-Kour shear zone summarized on a Flinn diagram.

positive and negative space with a set of semihyperbolas at 0.025 intervals of W_m, and parameter B^* is estimated by converting these curves into vertical lines. B^* indicates the critical value (R_c) separating grains that reach a stable-sink position from those that undergo continuous rotation during progressive deformation (Jessup et al., 2007). The mathematical relationship between the R_c and W_m can be defined as follows (Passchier, 1987):

$$W_m = (R_c^2 - 1).(R_c^2 + 1)^{-1} \quad \text{(eq. 3)}$$

W_m can be calculated from B*, since B* is equal to W_m. The shape factor of each clast is used here as presented by Jessup et al. (2007):

$$B^* = (M_x^2 - M_n^2)/(M_x^2 + M_n^2) \quad \text{(eq. 4)}$$

where Mx and Mn are the lengths of the long and short axes of the porphyroclast, respectively. The following assumptions have been considered in the application of the rigid-grain technique: (1) the porphyroclasts have not undergone internal deformation, and are harder than the surrounding matrix (Iacopini et al., 2011), (2) the porphyroclasts predate the fabrics formed during the deformation episode, (3) no slipping or interaction between adjacent clasts or with the matrix has occurred during the deformation (Passchier, 1987), and (4) the porphyroclasts are enclosed in a homogeneous matrix (Jessup et al., 2007). We applied the RGN technique to 11 oriented samples. The axial ratio and acute angle (Φ) between the long axis of feldspar porphyroclasts and the mylonitic foliation were measured (Figure 6).

4.4. Vertical thinning and dip-parallel elongation

In plane strain deformation, stretching parallel to the flow plane ($S^{-}1$) in the transport direction is the reciprocal of the shortening value (Law, 2010). Wallis et al. (1993, 1995) proposed a mathematical expression combining vorticity (W_m) and strain (R_{XZ}) data to calculate the stretch value vertical to the shear zone boundary (S).

$$S=\left\{\frac{1}{2}(1-W_m^2)^{1/2}\left[\left(R_{XZ}+R_{XZ}^{-1}+2\frac{(1+W_m^2)}{(1-W_m^2)}\right)^{1/2}+(R_{XZ}+R_{XZ}^{-1}-2)^{1/2}\right]\right\}^{-1} \quad \text{(eq. 5)}$$

5. Results

5.1. Micro- and mesostructural analysis of sheared lithotypes

The Chai-Kour shear zone is 15 km at its widest point and extends for several kilometers. Most of the shear zones contain structural features that formed during the exhumation of metamorphic rocks. In these metamorphic sections, the stretching lineations are gently plunging and dominated by stretched quartz and feldspar minerals. Well-developed mylonitic foliation is formed by silicates and flattened and stretched grains. Based on deformation temperature estimates and mineral assemblages, mylonitization occurred under upper greenschist- to amphibolite-facies metamorphic conditions, corresponding to temperatures of approximately 450–650 °C. Protomylonites and mylonites contain abundant feldspar and quartz porphyroclasts within a fine-grain matrix. Quartz displays grain boundary migration (GBM) and subgrain rotation (SGR) recrystallization, but only minor effects of dynamic bulging (BLG) in mylonites. Several kinematic indicators at meso and microscopic scales confirm the top-to-the-southeast shearing.

5.2. Finite strain analysis

The strain ratio (R_{XZ}) for the mylonitic sample in the study area ranges from 2.24 to 4.52 (Table 1). The highest estimated R_{XZ} values (samples Ck1 and Ck11, 4.20 and 4.52, respectively) are all close to the shear zone boundaries. Our three-dimensional strain analysis revealed most samples to be concentrated in the plane-strain field, while a few plots were in the prolate field (Figure 5). It was noted that Rxz values decrease as the distance from the shear zone boundaries increases (Table 1). The identified k-values range from 0.72 to 1.13 with an average of 0.92. Nadal (1963) defined strain intensity based on the octahedral shear strain parameter (εs). In the selected samples, εs varies from 0.57 to 1.01, with an average of 0.82.

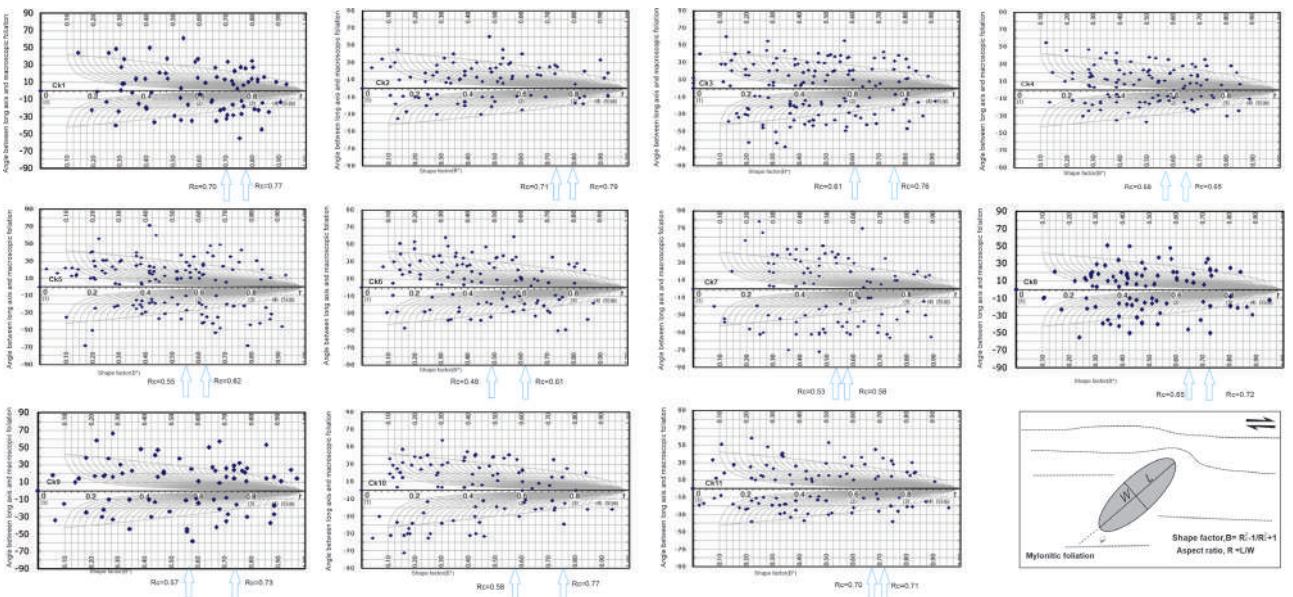

Figure 6. Rigid Grain Net for calculated kinmatic vorticity number (Jessup et al., 2007) by plots of shape factor, B*, vs. the angle Φ. Locations of sample in Fig. 2b.

5.3. Kinematic vorticity results

Using the RGN method, W_m maximum and minimum values fall within the 0.54–0.73 range (average W_m = 0.64) as exhibited in Table 2 and plotted in Figure 7. Specifically, calculated W_m values along the northeast–southwest transect exhibit a small but progressive increase toward the shear zone boundaries (Table 2, Figure 8a). The highest W_m values were found in samples taken from the northeast and southwest boundaries of the shear zone. In contrast, samples Ck5–Ck7, obtained from the central part of the shear zone, yield W_m values of 0.58, 0.54, and 0.55, respectively. The estimated W_k indicates a subsimple shear (Figure 8a).

Additionally, W_k was converted to a linear scale following Forte and Bailey (2007) for the estimation of the percentage of simple shear. In this classification, $W_k > 0.95$ corresponds to a simple shear-dominated deformation in which simple shear accounted for more than 80% of the total, whereas W_k = 0.3 corresponds to pure shear-dominated deformation with <20% simple shear. General shear deformation is represented by W_k values in the 0.3–0.95 range. Figure 8b presents the W_k values from the 11 samples and the variation of W_m within the Chai-Kour shear zone. The estimated percentages of the simple and pure shear components are in the ranges of 36–52%, and 64–48%, respectively.

5.4. Vertical thinning and dip-parallel elongation

The percentage of vertical shortening/thinning (S) and transport-parallel stretching (S^{-1}) can be calculated using W_m, Rxz and the numerical relationships reported by Wallis et al. (1993). Assuming constant-volume deformation, the vertical shortening estimates for all samples are in the region of 55–75%, varying with structural position along the northeast–southwest transect (Table 2, Figure 9a).

6. Discussion

6.1. progressive shearing and strain partitioning

The results of strain measurements and kinematic vorticity analyses are used to reconstruct the deformation history of the Chai-Kour Shear Zone within the Sanandaj-Sirjan metamorphic belt. Studies of extracted kinematic parameters, strain, and vorticity, and their distribution in ductile shear zones provide insights into the large-scale kinematic evolution of deformed terrains (Johnson et al., 2009; Roy and Matin, 2020).

The kinematic vorticity data and strain analysis derived from rotated porphyroclasts allowed us to quantify the deformation, which is characterized by plane strain and noncoaxial flow, comprising pure (46–62%) and simple (38–54%) shear components. These results confirm the spatial variation of strain during deformation, with simple shear dominating at the boundaries, and progressively decreasing toward the central parts of the shear zone (Figure 8b).

The deformation history of the Chai-Kour shear zone, characterized initially by high temperatures (550–650 °C) followed by a period of lower temperatures (380–420 °C), mirrors the polyphase metamorphism and deformation

Table 2. Results of W_k (Jessup et al., 2007) and stretching (S, Wallis et al., 1993) analyses on rotated K-feldspar porphyroclats in the Chai-Kour shear zone.

Sample	$R_{c(max)}$-$R_{c(min)}$	W_m	Pure shear (%)	Simple shear (%)	S
Ck1	0.70-0.77	0.73	46	54	0.61
Ck2	0.62-0.80	0.72	47	53	0.63
Ck3	0.61-0.76	0.69	51	49	0.69
Ck4	0.58-0.65	0.61	57	43	0.65
Ck5	0.55-0.62	0.58	59	41	0.75
Ck6	0.48-0.61	0.54	61	39	0.71
Ck7	0.53-0.58	0.55	62	38	0.60
Ck8	0.65-0.72	0.68	52	48	0.69
Ck9	0.57-0.73	0.65	54	46	0.57
Ck10	0.58-0.77	0.67	53	47	0.58
Ck11	0.70-0.71	0.70	49	51	0.55

Note: All parameters are unitless.
Maximum critical axial ratio ($R_{c(max)}$)
Mean critical axial ratio ($R_{c(min)}$)
Mean value of W_k (W_m)

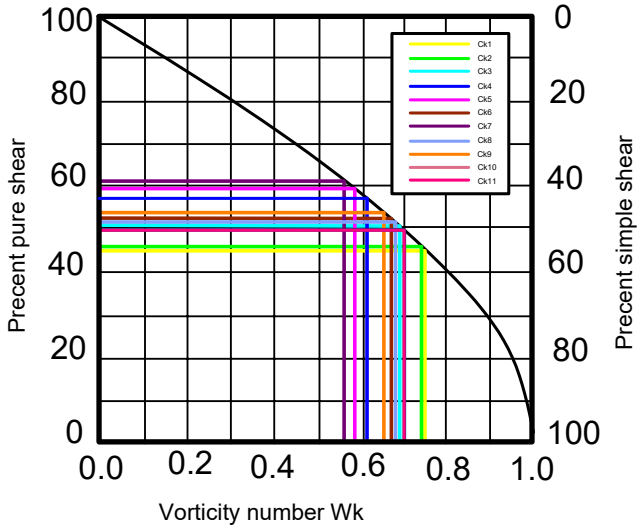

Figure 7. Diagram showing percentage of shear components in relation to measured kinematic vorticity number (W_k). Studied samples from the Chai-Kour shear zone presented in different colors.

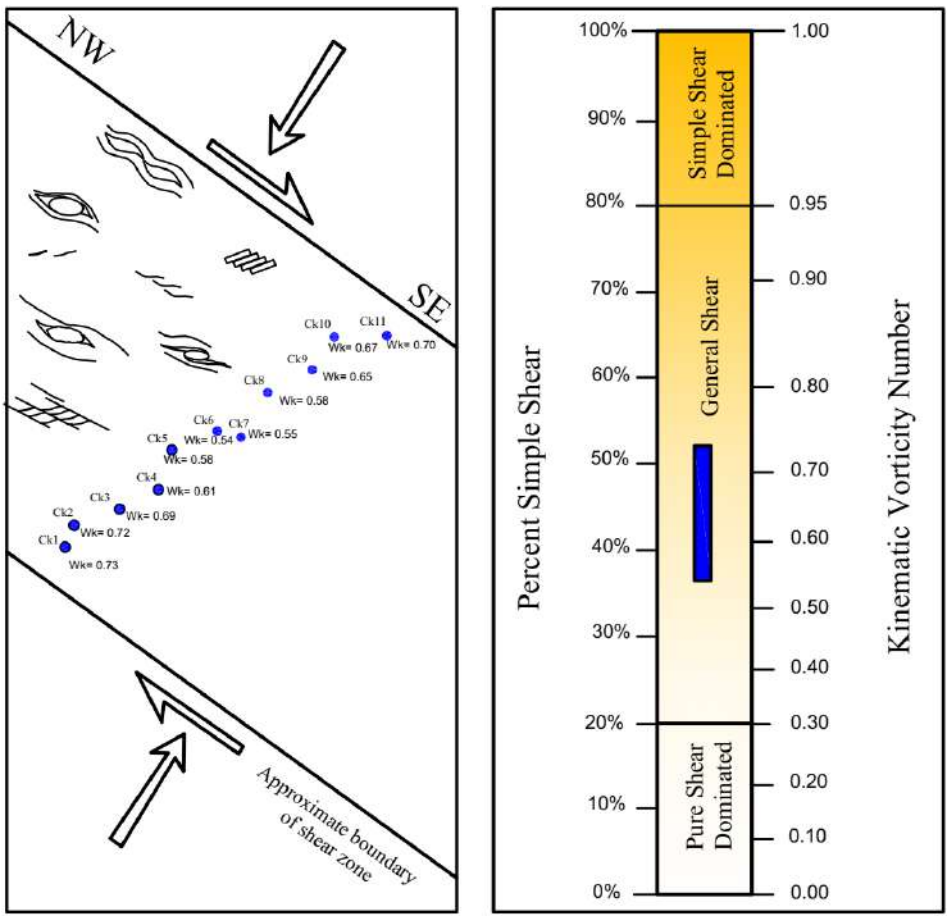

Figure 8. (a) Schematic diagram illustrating the sample locations across the Chai-Kour shear zone and their related W_k values, acquired through the RGN method. (b) Linear diagram showing the relationship between the W_m and simple shear percentage (modified after Forte and Bailey, 2007). Blue bar represents W_k of this study.

recorded elsewhere along the Sanandaj-Sirjan belt (Fergusson et al., 2016). This thermal evolution reflects the progressive exhumation of midcrustal rocks during the orogen's evolution (Langille et al. 2010; Law 2014; Simonetti et al., 2020b; Tiwari et al., 2020). The presence of quartz microstructures, indicative of grain boundary migration (GBM) and subgrain rotation (SGR), along with the bulging recrystallization (BLG) and the presence of brittle feldspar fractures, further supports the transition from deep-seated ductile deformation to shallower brittle-ductile conditions.

Additionally, the observation of well-developed meso- and microscale structures (e.g., shear bands, porphyroclast trails, crenulation cleavages, and stretching lineation with moderate to gently plunging) suggests a strong component of shortening, besides foliation-parallel shear (e.g. Grujic et al., 2002; Law et al., 2004; Vannay et al., 2004; Carosi et al., 2006; Godin et al., 2006; Grujic, 2006). Our results concur with those of previous studies in the literature adopting a vorticity analysis approach to the investigation of the spatial variations of strain in different ductile shear zones (see Table 3 for detailed references).

6.2. Transpression and crustal-scale tectonics

To distinguish between the transpression and transtension deformation types, in the present study, we estimated the angle Θ between the maximum instantaneous stretching axis (ISA_{max}) and the shear zone boundary (Tikoff and Fossen, 1995, Figure 9b) using the equation (Xypolias, 2010):

$$\theta = 0.5^{*}Sin^{-1}W_m \qquad \text{(eq. 6)}$$

The calculated Θ values are in the range of 16°–23°, which according to the diagram defining relationship between vorticity number and Θ angle (Ramsay and Graham, 1970; Tikoff and Fossen, 1993, 1995; Fossen and Cavalcante, 2017), corresponds to pure shear-dominated transpression (Figure 9b). Pure shear-dominated transpressional settings, (L)S fabrics typically develop with oblique foliations and vertical lineations (Fossen et al., 1994). The orientations of the stretching lineation distinguish the two end members of transpressive shear zones (Iacopini et al., 2008), with subvertical lineations indicating the shear zone experienced vertical extrusion, while subhorizontal lineations reflect horizontal extrusions.

The stretching lineation within the Chai-Kour shear zone plunges gently, indicating a lateral direction of extrusion. Jones et al. (1997) presented a theoretical analysis describing lateral extrusions in unconfined transpressional or transtensional shear zones, and reported that under specific conditions, the pure shear component leads to an unavoidable extensional strain parallel to the shear zone boundaries (lateral extrusion). Based on the results of analog experiments, Czeck and Hudleston (2004) modeled a transpression zone with localized, nonvertical extrusion, and demonstrated that the obliquity of the lineation is primarily dependent of the extrusion direction. The spatial variation in vorticity and strain suggests that the Chai-Kour shear zone has experienced both vertical thinning and lateral flow in its history, reflecting a combination of transpressional deformation and lateral extrusion (Sanderson and Marchini, 1984; Beaumont et al., 2001).

6.3. Broader implications for Zagros orogenesis

The deformation characteristics documented in the Chai-Kour shear zone provide critical insights into the larger-scale tectonic evolution of the Zagros orogen. The Zagros orogen, as part of the Alpine-Himalayan belt, has a complex history of subduction, collision, and post-collisional deformation since the Late Cretaceous (Agard et al., 2005). The Sanandaj-Sirjan metamorphic belt on which the Chai-Kour shear zone is located is key segment of the Zagros orogen containing evidence of the midcrustal deformation that occurred during the collision. The spatial variation in strain and vorticity, as well as the dominance of pure shear-dominated transpression, confirm the heterogeneous nature of the convergence regime. The Chai-Kour shear zone's gently plunging stretching lineations and pure shear-dominated transpression are indicative of a lateral extrusion—a common feature of unconfined transpressive zones (Jones et al., 1997, 2004; Czeck and Hudleston, 2004; Fernandez and Díaz-Azpiroz, 2009; Massey and Moecher, 2013). This mechanism is particularly relevant in the Zagros orogen, where the oblique convergence of the Afro-Arabian plate has led to the development of northwest–southeast trending shear zones and thrust faults, facilitating both crustal thickening and the extrusion of metamorphic rocks (Sarkarinejad et al., 2008; Partabian and Faghih, 2021). The estimated 55–75% vertical shortening in the Chai-Kour shear zone underscores the significance of crustal thickening during deformation. These findings align with existing records of strain partitioning in transpressive orogens, where crustal thickening and lateral flow are driven by the interplay of pure and simple shear components (Sanderson and Marchini, 1984; Tikoff and Fossen, 1993; Jones et al., 1997; Sarkarinejad et al., 2008; Tiwari et al., 2020). The increase in strain values toward the northeast and southwest boundaries of the Chai-Kour shear zone suggests strain localization along the major thrust systems, consistent with the broader architecture of the Sanandaj-Sirjan belt as a metamorphic core within the Zagros orogen (Sheikholeslami et al., 2019; Madanipour et al., 2024). Some metamorphic complexes are arranged parallel to the strike of the Zagros orogen, bordered by distinct ductile northwest–southeast-trending shear zones and thrusts. Our study of the Chai-Kour shear zone indicates the presence of a similar tectonic style, supported

Table 3. List of terrains, vorticity method, results of analysis, orogen and countries of several references, for comparison with results of the present study regarding to the variation of strain in the ductile shear zone.

Terrains	Vorticity method	Results of study	Orogen	Country	Reference
Main Central Thrust Zone	quartz textures	This study confirms spatial and temporal variation of deformation in ductile shear zone.	NW-Himalaya	India	Grasemann et al. (1999)
Mount Everest Massif	porphyroclast-based methods	Results suggest that the low-viscosity midchannel deformed by general shear with an increasing component of pure shear towards the center.	Tibet	Nepal	Jessup et al. (2006)
Albione Raft River shear zone	porphyroclast-based methods Quartz c-axis fabric	This study shows that samples collected from the basal cobble metaconglomerate yield significantly lower Wk values than those collected from the overlying quartzite mylonites, and these are the only samples that experienced a pure shear-dominated deformation history.	Grouse Creek metamorphic core complex	USA	Sullivan (2008)
Evia and Ochi thrust zones	porphyroclast-based methods Quartz c-axis fabric	The vorticity profile above the thrust plane shows a slight down-section increase in the kinematic vorticity number (Wm) from 0.8 to 0.9, as well as the presence of local thin domains with a higher pure shear component of deformation.	Alpine orogenic belt	Greece	Xypolias et al. (2010)
Ama Drime detachment	porphyroclast-based methods Quartz c-axis fabric	An increasing pure shear component with structural depth, and increasing deformation temperatures towards the middle of the dome.	Tibet	Nepal	Langille et al. (2010)
Moine thrust zone	porphyroclast-based methods Quartz c-axis fabric	A small but systematic decrease in estimated Wm value is detected with increasing distance beneath the thrust plane.	Himalayan	Stack of Glencoul	Law (2010)
Loch Eriboll area	porphyroclast-based methods Quartz c-axis fabric	An increase in noncoaxial deformation traced towards structurally higher levels, which is accompanied by increases in deformation temperature.	Scandian orogenic wedge	NW Scotland	Thigpen et al. (2010)
Neyriz shear zone	Quartz c-axis fabric	The results of this study demonstrate that both strain ratio and the simple shear component of deformation increase towards the basal thrust of the Zagros Thrust System.	Zagros orogen	Iran	Faghih and Sarkarinejad, (2011)
Rosy Finch Shear Zone	Quartz c-axis fabric	Vorticity analyses indicate that there is a significant component of pure shear deformation within this zone, ~75%. This pure shear component is responsible for ≈20% of horizontal shortening across this zone.	the Sierra Nevada Mountain range		Mookerjee et al. (2016)
Karakoram Shear Zone	porphyroclast-based methods Shear Band (SB) Analysis	The results indicate distinct pure and simple shear dominant regimes during different stages of the evolution of the KSZ.	Pangong Mountains	India	Roy et al. (2016)
Ailao Shan-Red River shear zone	porphyroclast-based methods Quartz c-axis fabric	The results show an obvious drop in Wk values calculated using quartz c-axis-fabric toward the middle of the shear zone may also indicate that late-stage simple shearing along the shear zone is nonhomogeneous.	SE Tibetan plateau	China	Wu et al. (2017)

Table 3. (Continued).

Atalla Shear zone	porphyroclast-based methods	The strain and vorticity analyses of Atalla shear zone indicate that these zones experienced general shear conditions.	East African Orogen	Egypt	Mohammad et al. (2020)
Ambaji granulite	porphyroclast-based methods	The results show the strain path of the exhumation of the granulites based on the kinematic vorticity to reconstruct temporal and spatial variation of strain in shear zones.	northwestern part of the Indian Peninsula	India	Tiwari et al. (2020)
Heneshk metamorphic rocks	porphyroclast-based methods	The results show higher amounts of *W*k near the major thrust faults and lower amounts of *W*k far from them.	Zagros orogen	Iran	Samani et al. (2020)
Aiguilles Rouges Massif	C' shear band porphyroclast-based methods	Kinematic vorticity analysis allows us to reveal that deformation along the Cavalaire "Fault" occurred under general shear condition with a major component of pure shear acting together with simple shear.	Variscan belt	France	Simonetti et al. (2020a)
Gol-e-Gohar metamorphic complex	porphyroclast-based methods Quartz c-axis fabric	This study proposed different amounts of strain, vorticity and strain partitioning in various parts of this deformed area.	Zagros orogen	Iran	Keshavarz and Faghih, (2020)
Alaknanda–Dhauli Ganga Valleys	porphyroclast-based methods	The analysis reveals that pure shear provides significant contribution (30–52%) to the deformation associated with southward ductile shearing along the MCT, with the highest mean kinematic vorticity number (Wm) values close to the MCT.	Uttarakhand Himalaya	India	Kanyan et al. (2021)
Darizhun shear zone	porphyroclast-based methods	The *W*m estimates demonstrate general shear deformation with gradual increase in the simple-shear component towards the Darizhan thrust sheet.	Zagros orogen	Iran	Derikvand, (2021)
Kahdan shear zone	porphyroclast-based methods	The results show a nonunified spatial variation of vorticity and strain values in the deformed metasandstone.	Zagros orogen	Iran	Shafiei bafti et al. (2022)
Qilian orogen	porphyroclast-based methods Quartz c-axis fabric	Considering kinematic vorticity analyses, finite strain, and structural orientation, this study indicates macroscale strain partitioning in a transpressional setting.	northern Tibet	China	Wu et al. (2023)
Xiaoqinling region	porphyroclast-based methods Quartz c-axis fabric	Vorticity analysis confirms simple-shear-dominated general-shear deformation within the shear zones, with an increase in a pure shear component during the later stages.	Trans-North China Orogen	China	Li et al. (2024)
Wildhorse Detachment system	Quartz c-axis fabric C′-type shear bands (C′-c) methods	This paper clarifies the spatial relationships and timing of deformation related to emplacement and exhumation of metamorphic core complexes.	North American Cordillera	Idaho	McFadden et al. (2024)

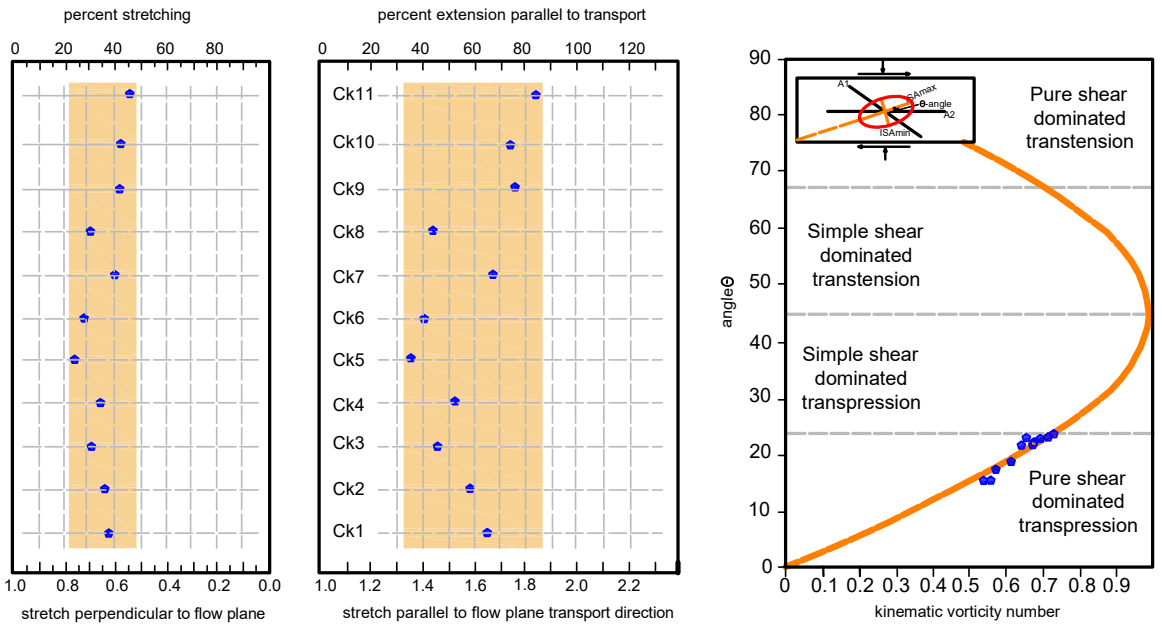

Figure 9. (a) Calculation of thinning/stretching values vs. structural distance relative to the shear zone boundaries. (b) Relationships between ISAmax and angle θ, related to the kinematic vorticity number W_k (modified from Fossen et al., 1994; Fossen and Tikoff 1993). All yielded values from this study fall within the pure shear-dominated transpression field.

by the findings of the innovative strain and temperature analysis of midcrustal shear zones in the Zagros orogen. The Neyriz area conforms to the models of Dewey et al. (1998), which involve both vertical and horizontal stretch components in unconfined transpression with lateral extrusion (Sarkarinejad et al., 2008). In other parts, the vertical extrusion of the gneiss core in the Chah-Sabz antiform resulted from dextral transpression (Partabian and Faghih, 2021). The strain ratio and the simple shear component of deformation recorded in the Dehbid area increase toward the basal thrust of the Zagros Thrust System (Sarkarinejad et al., 2010). The Qolqoleh-Kasnazan shear zone is constricted and prolate, indicating that deformation occurred under pure shear transtensional conditions (Behyari and Shahbazi, 2019).

6.4. Comparative context with global orogens

The results of this research underline the need to study regional shear zones with a multidisciplinary approach, and reinforce the role of shear zones as archives of progressive orogenic evolution. The recorded variations in strain, temperature, and kinematic patterns during transpressive deformation with lateral extrusions and crustal thinning in the Chai-Kour shear zone are consistent with those observed in other deformed zones in various orogenic belts (Table 3, England and Houseman, 1986; Law et al., 2004, 2010; Nabavi et al., 2017; Simonetti et al., 2020a; Tiwari et al., 2020; Cheng et al., 2022). In Himalayan tectonics, crustal thickening of the Tibetan Plateau and lateral extrusions in the Southeast Asian region have been reported (Replumaz and Tapponnier, 2003). In the Ambaji granulite in northwest India, strain partitioning with vertical displacement and crustal thickening in a large-scale thrust tectonic setting has been noted, followed by lateral migration of the granulite (Tiwari et al., 2020). The Aiguilles Rouges Massif in the Western Alps is a dextral, pure shear-dominated transpression zone created under amphibolite-facies metamorphic conditions (Simonetti et al., 2020b).

7. Conclusions

The Chai-Kour shear zone exemplifies how localized deformation processes serve as a record of the broader tectonic history of continental collision, offering a window into the mechanics of crustal-scale strain accommodation and the evolution of orogenic systems. This shear zone documents polyphase deformation under amphibolite- to upper-greenschist facies conditions (550–420 °C), with kinematic indicators revealing top-to-the-southeast shearing. The presence of quartz microstructures created under different temperature conditions indicates that the flow of the rocks changed from early higher- to late lower-temperature shear. Strain analysis reveals plane-strain to prolate deformation (R_{XZ}= 2.24–4.52), with maximum values occurring near the shear zone boundaries. Vorticity estimates (W_m= 0.54–0.73) indicate the presence of a subsimple shear regime exhibiting increased simple shear components (38–54%) toward the margins. The 16°–23° angular relationship between ISAmax and the shear zone boundaries, coupled with gently plunging

stretching lineations (15°–30°), confirms pure shear-dominated transpression with significant lateral extrusion components. These findings demonstrate how the strain partitioning mechanisms accommodated continental collision in the Zagros orogen, where transpression and lateral extrusion facilitated crustal thickening and metamorphic exhumation. They also allow valuable comparisons with other collisional systems, such as the Alpine and Himalayan orogens. This study highlights the role of shear zones in crustal thickening, and establishes a framework for understanding midcrustal deformations in orogens. Future studies should include geochronological analyses to better clarify the deformation timing.

Acknowledgements
This research has been supported by Institute of Science and High Technology and Environmental Science, Graduate University of Advanced Technology. The authors express their gratitude to J.E. Saylor and an anonymous reviewer for their critical comments and constructive reviews, which improved the quality of the manuscript. They further give thanks to the editor of the journal for their helpful comments and handling of the manuscript.

Author Contributions
Saeede KESHAVARZ: conceptualization, data curation, formal analysis, methodology, project administration, software, writing – review & editing)
Saeed ZAREI: conceptualization, data curation, formal analysis, software, writing – original draft.
Majid SHAHPASANDZADEH: conceptualization, formal analysis, methodology, writing – original draft.
Soumyajit MUKHERJEE: validation, draft finalization – review & editing.

References

Agard P, Omrani J, Jolivet L, Mouthereau F (2005). Convergence history across Zagros (Iran): Constraints from collisional and earlier deformation. International Journal of Earth Sciences 94: 401-419. https://doi.org/10.1007/s00531-005-0481-4

Agard P, Omrani J, Jolivet L, Whitechurch H, Vrielynck B et al. (2011). Zagros orogeny: a subduction- dominated process. Geological Magazine 148: 692–725. https://doi.org/10.1017/S001675681100046X

Alavi M (2004). Regional stratigraphy of the Zagros fold-thrust belt of Iran, and its proforeland evolution. American Journal of Science 304: 1–20. https://doi.org/10.2475/ajs.304.1.1

Allen M, Jackson J, Walker R (2004). Late Cenozoic reorganization of the Arabia–Eurasia collision and comparison of the short-term and long-term deformation rates. Tectonics 23: TC2008. https://doi.org/10.1029/2003TC001530

Beaumont C, Jamieson RA, Nguyen MH, Lee B (2001). Himalayan tectonics explained by Moıne Thrust Zone Mylonıtes At The Stack Of Glencoul: II extrusion of a low-viscosity crustal channel coupled to focused surface denudation. Nature 414: 738–742. https://doi.org/10.1038/414738a

Behyari M, Shahbazi M (2019). Strain and vorticity analysis in the Zagros suture zone (W Iran): implications for Neo-Tethys postcollision events. Journal of Structural Geology 126: 198–209. https://doi.org/10.1016/j.jsg.2019.06.002

Bose N, Dutta D, **Mukherjee S** (2018). Role of grain-size in phyllonitisation: Insights from mineralogy, microstructures, strain analyses and numerical modeling. Journal of Structural Geology 112: 39–52. https://doi.org/10.1016/j.jsg.2018.03.010

Bose N, **Mukherjee S** (2020). Estimation of deformation temperatures, flow stresses and strain rates from an intra-continental shear zone: the Main Boundary Thrust, NW Himalaya (Uttarakhand, India). Marine and Petroleum Geology 112: 104. https://doi.org/10.1016/j.marpetgeo.2019.104094

Carosi R, Montomoli C, Rubatto D, Visoná D (2006). Normal-sense shear zones in the core of the Higher Himalayan Crystallines (Bhutan Himalaya); evidence for extrusion? In: Law, R.D, Searle, M.P, Godin, L. (Eds.), Channel flow, Ductile Extrusion and Exhumation in Continental Collision Zones. Geological Society, London, Special Publication 268: 425–444. https://doi.org/10.1144/GSL.SP.2006.268.01.20

Carreras J, Cosgrove JW, Druguet E (2013). Strain partitioning in banded and/or anisotropic rocks: Implications for inferring tectonic regimes. Journal of Structural Geology 50, pp. 7–21.

Cheng CH, Sun SH, Dong Y, Zhang B, Guo Z (2022). Exhumation of plutons controlled by boundary faults: Insights from the kinematics, microfabric, and geochronology of the Taibai shear zone, Qinling Orogen, China. GSA Bulletin 134 (11-12): 2723–2744. https://doi.org/10.1130/B36073.1

Chew DM (2003). An excel spreadsheet for finite strain analysis using the Rf/Φ technique. Computer Geoscience 29: 795–799. https://doi.org/10.1016/S0098-3004(03)00027-X

Czeck DM, Hudleston PJ (2004). Physical experiments of vertical transpression with localized nonvertical extrusion. Journal of Structural Geology 26: 573–581. https://doi.org/10.1016/j.jsg.2003.07.002

Derikvand S (2021). Quantitative kinematic analyses of the Darizhun shear zone within the hinterland of the Zagros orogenic belt, Iran. International Journal of Earth Sciences 110: 609–626. https://doi.org/10.1007/s00531-020-01976-9

Derikvand S, Almasi A (2022). Kinematic vorticity, finite strain, and deformation thermometry analyses of the exhumed mylonites in the Samen ductile shear zone (Sanandaj-Sirjan Metamorphic Belt, Iran). Journal of Structural Geology 104500. https://doi.org/10.1016/j.jsg.2021.104500

Dewey JF, Holdsworth RE, Strachan RA (1998). Transpression and transtension zones, 135. Geological Society, London, Special Publications 1–14. https://doi.org/10.1144/gsl.sp.1998.135.01.01

Dias R, Coke C, Ribeiro A (2022). Strain partitioning in the Variscan deformation of the Marão domain (Central Iberian zone; northern Portugal). Journal of Structural Geology 161, p.104635. https://doi.org/10.1016/j.jsg.2022.104635

Díaz-Azpiroz M, Barcos, Balanyá J C, Fernández CF, Czeck DM (2016). Tectonics of oblique plate boundary systems. Ectonophysics 693: 165–170. https://doi.org/10.1016/j.tecto.2016.07.028

England P, Houseman G (1986). Finite strain calculations of continental deformation: Comparison with the India-Asia collision zone. Journal of Geophysical Research: Solid Earth 91: 3664-3676. https://doi.org/10.1029/JB091iB03p03664

Faghih A, Sarkarinejad K (2011). Kinematics of rock flow and fabric development associated with shear deformation within the Zagros transpression zone, Iran. In: Lacombe O, Grasemann B, Simpson G (eds) Geodynamic evolution of the Zagros. Geological Magazine 148: 1009–1017. https://doi.org/10.1017/S0016756811000276

Faghih A, Soleimani M (2015). Quartz c-axis fabric development associated with shear deformation along an extensional detachment shear zone: chapedony Metamorphic Core Complex, Central East Iranian Microcontinent. Journal of Structural Geology 70: 1–11. https://doi.org/10.1016/j.jsg.2014.10.016

Fergusson C, Nutman AP, Mohajjel M, Bennett V (2016). The Sanandaj-Sirjan Zone in the Neo-Tethyan suture, western Iran: Zircon U-Pb evidence of late Palaeozoic rifting of northern Gondwana and mid-Jurassic orogenesis. Gondwana Research 40: 43–57. https://doi.org/10.1016/j.gr.2016.08.006

Fernandez C, Diaz-Azpiroz M (2009). Triclinic transpression zones with inclined extrusion. Journal of Structural Geology 31: 1255–1269. https://doi.org/10.1016/j.jsg.2009.07.001

Flinn D (1962). On folding during three-dimensional progressive deformation. Quarterly Journal of the Geological Society 118: 385–428. https://doi.org/10.1144/gsjgs.118.1.0385

Flinn D (1978). The construction and computation of three-dimensional progressive deformations. Journal of the Geological Society of London 135: 291–305. https://doi.org/10.1144/gsjgs.135.3.0291

Forte AM, Bailey CM (2007). Testing the utility of the porphyroclast hyperbolic distribution method of kinematic vorticity analysis. Journal of Structural Geology 29: 983–1001. https://doi.org/10.1016/j.jsg.2007.01.006

Fossen H (2016). Structural geology. Cambridge University Press, Cambridge, p 524

Fossen H, Basil T, Christian T (1994). Strain modeling of transpressional and transtensional deformation. Norsk Geologisk Tidsskrift 74: 134–145.

Fossen H, Cavalcante GCG (2017). Shear zones A review: Earth-Science Reviews 171: 434–455. https://doi.org/10.1016/j.earscirev.2017.05.002

Frassi C, Carosi R, Montomoli C, Law RD (2009). Kinematics and vorticity of flow associated with post-collisional oblique transpression in the Variscan Inner Zone of northern Sardinia (Italy). Journal of Structural Geology 31: 1458–1471. https://doi.org/10.1016/j.jsg.2009.10.001

Goscombe BD, Passchier CW, Hand M (2004). Boudinage classification: end-member boudin types and modified boudin structures. Journal of Structural Geology 26 (4): 739–763. https://doi.org/10.1016/j.jsg.2003.08.015

Grasemann B, Fritz H, Vannay JC (1999). Quantitative kinematic flow analysis from the Main Central Thrust Zone (NW-Himalaya, India): implications for a decelerating strain path and the extrusion of orogenic wedges. Journal of Structural Geology 21: 837–853. https://doi.org/10.1016/S0191-8141(99)00077-2

Grujic D (2006). Channel flow and continental collision tectonics; an overview. In: Law, R.D, Searle, M.P, Godin, L. (Eds.), Channel Flow, Ductile Extrusion and Exhumation in Continental Collision Zones. Geological Society, London, Special Publication 268: 25–37. https://doi.org/10.1144/GSL.SP.2006.268.01.02

Grujic D, Hollister LS, Parrish RR (2002). Himalayan metamorphic sequence as an orogenic channel: insight from Bhutan. Earth and Planetary Letters 198: 177–191. https://doi.org/10.1016/S0012-821X(02)00482-X

Jessell M, Lister GS (1990). A simulation of the temperature dependence of quartz fabrics. In: Knipe, R.J, Rutter, E.H. (Eds.), Deformation Mechanisms, Rheology and Tectonics. Geological Society, London, Special Publications 54: 353–362. https://doi.org/10.1144/GSL.SP.1990.054.01.31

Jessup MJ, Law RD, Frassi C (2007). The Rigid Grain Net (RGN): an alternativemethod for estimating mean kinematic vorticity number (Wm). Journal of Structural Geology 29: 411–421. https://doi.org/10.1016/j.jsg.2006.11.003

Jessup MJ, Law RD, Searle MP, Hubbard MS (2006). Structural evolution and vorticity of flow during extrusion and exhumation of the Greater Himalayan Slab, Mount Everest Massif, Tibet/Nepal: implications for orogen-scale flow partitioning. In: Law, RD, Searle, MP, Godin, L. (Eds.), Channel Flow, Ductile Extrusion and Exhumation in Continental Collision Zones. Geological Society,London, Special Publication 268: 379–413. https://doi.org/10.1144/GSL.SP.2006.268.01.18

Jiang D, Williams PF (1998). High-strain zones: a unifed model. Journal of Structural Geology, 20, 1105–1120. https://doi.org/10.1016/S0191-8141(98)00025-X

Passchier CW (1998). Monoclinic model shear zones. Journal of Structural Geology 20: 1121–1137. https://doi.org/10.1016/S0191-8141(98)00046-7

Johnson SE, Lenferink HJ, Price NA, Marsh JH, Koons PO (2009). Clast-based kinematic vorticity gauges: the effects of slip at matrix/clast interfaces. Journal of Structural Geology 31: 1322–1339. https://doi.org/10.1016/j.jsg.2009.07.008

Jones RR, Holdsworth RE, Clegg P, McCaffrey K, Tavarnelli E (2004). Inclined transpression. Journal of Structural Geology 26: 1531–1548. https://doi.org/10.1016/j.jsg.2004.01.004

Jones RR, Holdsworth RE, Bailey W (1997). Lateral extrusion in transpression zones: the importance of boundary conditions. Journal of Structural Geology 19: 1201–1217. https://doi.org/10.1016/S0191-8141(97)00034-5

Kanyan L, Jain AK, Singh S (2021). Vorticity patterns along the Main Central Thrust Zone, Alaknanda–Dhauli Ganga Valleys (Garhwal), Uttarakhand Himalaya. Journal of Earth System Science 130: 31. https://doi.org/10.1007/s12040-020-01539-1

Langille J, Lee J, Hacker B, Seward G (2010). Middle crustal ductile deformation patterns in southern Tibet: insights from vorticity studies in Mabja Dome. Journal of Structural Geology 32 (1): 70–85. https://doi.org/10.1016/j.jsg.2009.08.009

Law RD (2010). Moine thrust zone mylonites at the stack of Glencoul II: results of vorticity analyses and their tectonic significance. In: Law RD, Butler RWH, Holdsworth R, Krabbendam M, Strachan R (editors). Continental Tectonics and Mountain BuildingeThe Legacy of Peach and Horne. Geological Society, London, Special Publications 335: 359–381. https://doi.org/10.1144/sp335.24

Law RD (2014). Deformation thermometry based on quartz c-axis fabrics and recrystallization microstructures: a review. Journal of Structural Geology 66: 129–161. https://doi.org/10.1016/j.jsg.2014.05.023

Law RD, Mainprice D, Casey M, Lloyd GE, Knipe RJ et al. (2010). Moine thrust zone mylonites at the Stack of Glencoul: I–microstructures, strain and influence of recrystallization on quartz crystal fabric development. Geological Society, London, Special Publications 335: 543–577. https://doi.org/10.1144/SP335.23

Law RD, Searle MP, Simpson RL (2004). Strain, deformation temperatures and vorticity of flow at the top of the greater Himalayan Slab, Everest Massif, Tibet. Journal of Geological Society of London 161: 305–320. https://doi.org/10.1144/0016-764903-047

Li Y, Zhu G, Gu CH, Liu CH, Zhang S et al. (2023). Prolonged evolution of syn-collisional progressive deformation of the trans-north China orogen: structural and geochronological evidence from the Xiaoqinling region, Central China. Gondwana Research 129: 332–354. https://doi.org/10.1016/j.gr.2023.12.013

Madanipour S, Najafi M, Nozaem R, Vergés J, Yassaghi A et al. (2024). The Arabia–Eurasia Collision Zone in Iran: Tectonostratigraphic and Structural Synthesis. Journal of Petroleum Geology 47 (2): 123–171. https://doi.org/10.1111/jpg.12854

Mansouri SM, Keshavarz S, Shahpasandzadeh M, Faghih A (2021). Strain and vorticity analyses using rotated porphyroclasts in the Tanbour metamorphic rocks: Evidence of transpressional deformation along the Sanandaj–Sirjan metamorphic belt, SW Iran, Journal of Structural Geology 148: 104358. https://doi.org/10.1016/j.jsg.2021.104358

Mansouri SM, Keshavarz S, Shahpasandzadeh M, Faghih A (2023). Kinematics of the Tanbour Metamorphic Complex (SE Iran): Implications for Cenozoic Metamorphism and Deformation in the Northeastern Margin of the Afro-Arabian Plate. Geotectonics 57: 213–229. https://doi.org/10.1134/S001685212302005X

McFadden RR, Taylor JM, Whitney DL, Teyssier C, Seaton NCA et al. (2024). Deformation conditions and kinematic vorticity within the footwall shear zone of the Wildhorse detachment system, Pioneer metamorphic core complex, Idaho. Journal of Structural Geology 178: 105031. https://doi.org/10.1016/j.jsg.2023.105031

Massey M, Moecher DP (2013). Transpression, extrusion, partitioning, and lateral escape in the middle crust: Significance of structures, fabrics, and kinematics in the Bronson Hill zone, southern New England, U.S.A. Journal of Structural Geology 55: 62-78. https://doi.org/10.1016/j.jsg.2013.07.014

Meher B, Behera BM, Biswal TK (2020). Dynamic recrystallization mechanisms and vorticity estimation of the Terrane Boundary Shear Zone (Lakhna shear zone): Implications on dynamics of juxtaposition of the Eastern Ghats Mobile Belt with the Bastar Craton, NW Odisha. Journal of Earth System Science 129: 124. https://doi.org/10.1007/s12040-020-01393-1

Mohajjel M, Fergusson CL (2000). Dextral transpression in Late Cretaceous continental collision, Sanandaj-Sirjan zone, western Iran. Journal of Structural Geology 22: 1125–1139. https://doi.org/10.1016/S0191-8141(00)00023-7

Mohammad AT, El Kazzaz YA, Hassan SM, TAHA MMN (2020). Neoproterozoic tectonic evolution and exhumation history of transpressional shear zones in the East African orogen: implications from kinematic analysis of Meatiq area, Central Eastern Desert of Egypt. International Journal of Earth sciences (Geol Rundsch) 109: 253–279. https://doi.org/10.1007/s00531-019-01801-y

Montemagni C, Zanchetta S (2022). Constraining kinematic and temporal evolution of a normal-sense shear zone: Insights into the Simplon Shear Zone (Western Alps). Journal of Structural Geology 156, p.104557. https://doi.org/10.1016/j.jsg.2022.104557

Mookerjee M, Canada A, Fortescue FQ (2016). Quantifying thinning and extrusion associated with an oblique subduction zone: an example from the Rosy Finch Shear Zone. Tectonophysics 693 (4): 290–303. https://doi.org/10.1016/j.tecto.2016.06.012

Mouthereau F, Lacombe O, Vergés J (2012). Building the Zagros collisional orogen: timing, strain distribution and the dynamics of Arabia/Eurasia plate convergence. Tectonophysics 532: 27–60. https://doi.org/10.1016/j.tecto.2012.01.022

Mukherjee S (2011). Mineral Fish: their morphological classification, usefulness as shear sense indicators and genesis. International Journal of Earth Sciences 100: 1303–1314. https://doi.org/10.1007/s00531-010-0535-0

Mukherjee S (2013). Channel flow extrusion model to constrain dynamic viscosity and Prandtl number of the Higher Himalayan Shear Zone. International Journal of Earth Sciences 102: 1811–1835. https://doi.org/10.1007/s00531-012-0806-z

Mukherjee S (2017). Review on symmetric structures in ductile shear zones. International Journal of Earth Sciences 106: 1453–1468. https://doi.org/10.1007/s00531-016-1366-4

Mukherjee S (2019). Kinematics of pure shear ductile deformation within rigid walls: New analyses. In: Billi A, Fagereng A (editors). Problems and Solutions in Structural Geology and Tectonics. Series Editor: Mukherjee S. Developments in Structural Geology and Tectonics Book Series. Elsevier. pp. 81–88.

Mukherjee S (2012). Simple shear is not so simple! Kinematics and shear senses in Newtonian viscous simple shear zones. Geological Magazine 149: 819–826. https://doi.org/10.1017/S0016756811001075

Mukherjee S (2014). Review of flanking structures in meso- and micro-scales. Geological Magazine 151: 957–974. https://doi.org/10.1017/S0016756813001088

Mukherjee S, Biswas R (2014). Kinematics of horizontal simple shear zones of concentric arcs (Taylor–Couette flow) with incompressible Newtonian rheology. International Journal of Earth Sciences 103: 597–602. https://doi.org/10.1007/s00531-013-0973-6

Mukherjee S, Khonsari MM (2018). Inter-book normal fault-related shear heating in brittle bookshelf faults. Marine and Petroleum Geology 97: 45–48. https://doi.org/10.1016/j.marpetgeo.2018.06.029

Mukherjee S, Koyi HA (2010). Higher Himalayan Shear Zone, Sutlej section: structural geology and extrusion mechanism by various combinations of simple shear, pure shear and channel flow in shifting modes. International Journal of Earth Sciences 99: 1267–1303. https://doi.org/10.1007/s00531-009-0459-8

Mukherjee S, Punekar J, Mahadani T, Mukherjee R (2015). A review on intrafolial folds and their morphologies from the detachments of the western Indian Higher Himalaya.In: Mukherjee S, Mulchrone KF (Eds) Ductile Shear Zones: From Micro- to Macro-scales. Wiley Blackwell pp. 182 205. https://doi.org/10.1002/9781118844953.ch12

Nabavi ST, Díaz-Azpiroz M, Talbot CJ (2017). Inclined transpression in the neka valley, eastern Alborz, Iran. International Journal of Earth Sciences 106, pp.1815–1840. https://doi.org/10.1007/s00531-016-1388-y

Nabavi ST, Alavi SA, Díaz-Azpiroz M, Mohammadi S, Ghassemi MR et al. (2020). Deformation mechanics in inclined, brittle-ductile transpression zones: Insights from 3D finite element modelling. Journal of Structural Geology 137, p.104082. https://doi.org/10.1016/j.jsg.2020.104082

Nabavi ST, Alavi SA, Mohammadi S, Ghassemi MR (2018). Mechanical evolution of transpression zones affected by fault interactions: insights from 3D elasto-plastic finite element models. Journal of Structural Geology 106, pp. 19-40. https://doi.org/10.1016/j.jsg.2017.11.003

Nabavi ST, Fossen H (2021). Fold geometry and folding–a review. Earth-Science Reviews 222: 103812. https://doi.org/10.1016/j.earscirev.2021.103812

Partabian A, Faghih A (2021). Doming along the Zagros transpression zone, SW Iran: insights from microstructural analysis of heterogeneous deformation. Arabian Journal of Geosciences 14: 648. https://doi.org/10.1007/s12517-021-06835-8

Passchier CW (1987). Stable positions of rigid objects in non-coaxial flow—a study in vorticity analysis. Journal of Structural Geology 9: 679–690. https://doi.org/10.1016/0191-8141(87)90152-0

Passchier CW, Trouw RAJ (2005). Microtectonics. 2nd ed. Berlin, Germany: Springer.

Petroccia A, Carosi R, Montomoli C, Iaccarino S, Brovarone AV (2022). Deformation and temperature variation along thrust-sense shear zones in the hinterland-foreland transition zone of collisional settings: A case study from the Barbagia Thrust (Sardinia, Italy). Journal of Structural Geology 161: 104640. https://doi.org/10.1016/j.jsg.2022.104640

Petroccia A, Carosi R, Montomoli C, Iaccarino S, Forshaw JB et al. (2024). Transtension or transpression? Tectono-metamorphic constraints on the formation of the Monte Grighini dome (Sardinia, Italy) and implications for the Southern European Variscan belt. International Journal of Earth Sciences 113 (4): 797–820. https://doi.org/10.1007/s00531-024-02410-0

Ramberg H (1975). Particle paths, displacement and progressive strain applicable to rocks. Tectonophysics 28: 1–37. https://doi.org/10.1016/0040-1951(75)90058-X

Ramsay JG (1967) Folding and Fracturing of Rocks. New York, NY, USA: McGraw-Hill.

Ramsay JG, Graham RH (1970). Strain variation in shear belts: Canadian Journal of Earth Sciences 7: 786–813. https://doi.org/10.1139/e70-078

Roy A, Matin, A (2020). Study of small-scale structures and their significance in unravelling the accretionary character of Singhbhum shear zone, Jharkhand, India. Journal of Earth System Science 129: 227. https://doi.org/10.1007/s12040-020-01496-9

Roy P, Jain AK, Singh S (2016). Kinematic vorticity analysis along the Karakoram Shear Zone, Pangong Mountains, Karakoram: Implications for the India–Asia tectonics. Journal of Geological Society of India 87: 249–260. https://doi.org/10.1007/s12594-016-0392-y

Sadeghi A, Hakimi Asiabar S, Nezafati, N Mukherjee S (2023). Interaction between tectonics, plutonism and mineralization of the Duna Pb-Ba ore deposit regarding fluid inclusion study (Central Alborz, Iran). Acta Geologica Polonica 73: 201–222. https://doi.org/10.24425/agp.2022.143597

Samani B, Faghih A, Grasemann B (2020). Strain pattern and vorticity analysis of deformed conglomerates in the Heneshk area within the Sanandaj–Sirjan Metamorphic Belt, Zagros Mountains, Iran. International Journal of Earth Sciences 109: 145–157. https://doi.org/10.1007/s00531-019-01794-8

Sanderson DJ, Marchini WRD (1984). Transpression. Journal of Structural Geology 6: 449–458. https://doi.org/10.1016/0191-8141(84)90058-0

Sarkarinejad K, Azizi A (2008). Slip partitioning and inclined dextral transpression along the Zagros Thrust System, Iran. Journal of Structural Geology 30: 116–136. https://doi.org/10.1016/j.jsg.2007.10.001

Sarkarinejad K, Faghih A, Grasemann B (2008). Transpressional deformations within the Sanandaj-Sirjan metamorphic belt (Zagros Mountains, Iran). Journal of Structural Geology 30: 818–826. https://doi.org/10.1016/j.jsg.2008.03.003

Sarkarinejad K, Keshavarz S, Faghih A (2015). Strain Analysis in the Sanandaj-Sirjan HP-LT Metamorphic Belt, SW Iran: Insights from Small-Scale Faults and Associated Drag Folds. Journal of African Earth Sciences 105 (4): 47–54. https://doi.org/10.1016/j.jafrearsci.2015.02.006

Sarkarinejad K, Keshavarz S, Faghih A, Samani B (2017). Kinematic analysis of rock flow and deformation temperature of the Sirjan thrust sheet, Zagros Orogen, Iran. Geolohical magazine 154: 147–165. https://doi.org/10.1017/S0016756815000941

Sarkarinejad k, Laurent G, Faghih A (2009). Kinematic vorticity flow analysis and 40Ar-39Ar geochronology related to inclined extrusion of the HP–LT metamorphic rocks along the Zagros accretionary prism, Iran. Journal of Structural Geology 31: 691–706. https://doi.org/10.1016/j.jsg.2009.04.003

Shafiei bafti Sh, Keshavarz S, Zarei S (2022). Strain partitioning in the Kahdan shear zone: Microstructural and kinematic evidence from the SE Sanandaj-Sirjan zone, Zagros orogeny. Journal of Structural Geology 165: 104759. https://doi.org/10.1016/j.jsg.2022.104759

Sheikholeslami MR, Ghassemi MR, Hassanzadeh J (2019). Tectonic evolution of the hinterland of the Zagros Orogen revealed from the deformation of the Golpaygan Metamorphic Complex, Iran. Journal of Asian Earth Sciences 182: 103929. https://doi.org/10.1016/j.jseaes.2019.103929

Simonetti M, Carosi R, Montomoli C, Corsini M, Petroccia A et al. (2020a). Timing and kinematics of flow in a transpressive dextral shear zone, Maures Massif (Southern France). International Journal of Earth Sciences 109: 2261–2285. https://doi.org/10.1007/s00531-020-01898-6

Simonetti M, Carosi R, Montomoli, C, Cottle JM, Law RD (2020b). Transpressive deformation in the Southern European Variscan belt: new insights from the Aiguilles Rouges Massif (Western Alps). Tectonics 39. https://doi.org/10.1029/2020TC006153

Simpson C, De Paor D (1993). Strain and kinematic analysis in general shear zones. Journal of Structural Geology 15: 1-20. https://doi.org/10.1016/0191-8141(93)90075-L

Simpson C, De Paor DG (1997). Practical analysis of general shear zones using the porphyroclast hyperbolic distribution method: an example from the Scandinavian Caledonides. In: Sengupta, S. (Ed.), Evolution of Geological Structures in Micro- to Macro-Scales. Chapman and Hall 169–184. https://doi.org/10.1007/978-94-011-5870-1_10

Stipp M, Stünitz H, Heilbronner R, Schmid SM (2002a). The eastern Tonale fault zone: a 'natural laboratory' for crystal plastic deformation of quartz over a temperature range from 250 to 700 °C. Journal of Structural Geology 24: 1861–1884. https://doi.org/10.1016/S0191-8141(02)00035-4

Stipp M, Stünitz H, Heilbronner R, Schmid SM (2002b). Dynamic recrystallization of quartz: correlation between natural and experimental conditions. In: De Meer S, Drury MR, De Bresser JHP, Pennock GM (eds) Deformation mechanisms, rheology and tectonics: current status and future perspectives. Geological Society London, London, pp. 171–190. https://doi.org/10.1144/gsl.sp.2001.200.01.11

Stipp M, Tullis J, Scherwath M, Behrmann JH (2010). A new perspective on paleopiezometry: Dynamically recrystallized grain size distributions indicate mechanics changes. Geology 38: 759–762. https://doi.org/10.1130/G31162.1

Sullivan WA (2008). Significance of transport-parallel strain variations in part of the Raft River shear zone, Raft River Mountains, Utah, USA. Journal of Structural Geology 30: 138–158. https://doi.org/10.1016/j.jsg.2007.11.007

Thigpen RJ, Law RD, Lloyd GE, Brown SJ (2010). Deformation temperatures, vorticity of flow, and strain in the Moine thrust zone and Moine nappe: reassessing the tectonic evolution of the Scandian foreland-hinterland transition zone. Journal of Structural Geology 32 (7): 920–940. https://doi.org/10.1016/j.jsg.2010.05.001

Tikoff B, Fossen H (1995). The limitations of three-dimensional kinematic vorticity analysis. Journal of Structural Geology 12: 1771–1784. https://doi.org/10.1016/0191-8141(95)00069-P

Tikoff B, Fossen H (1993). Simultaneous pure and simple shear: the unifying deformation matrix. Tectonophysics 217: 267–283. https://doi.org/10.1016/0040-1951(93)90010-H

Tiwari SK, Beniest A, Biswal TK (2020). Variation in vorticity of flow during exhumation of lower crustal rocks (Neoproterozoic Ambaji granulite, NW India), Journal of Structural Geology 139: 103912. https://doi.org/10.1016/j.jsg.2019.103912

Tullis J (2002). Deformation of granitic rocks: Experimental studies and natural examples. In:Karato, S.I, Wenk, H.R. (Eds.), Plastic Deformation of Rocks and Minerals. Reviews in Mineralogy and Geochemistry 51: 51–95. https://doi.org/10.2138/gsrmg.51.1.51

Twiss RT, *Moores* EM (2006). Structural Geology. New York, NY, USA: W. H. Freeman & Co, San Francisco.

Vannay JC, Grasemann B, Rahn M, Fran W, Carter A et al. (2004. Miocene to Holocene exhumation of metamorphic crustal wedges in the NW Himalaya: Evidence for tectonic extrusion coupled to fluvial erosion. Tectonics 23. https://doi.org/10.1029/2002TC001429

Vergés J, Casini G, Ruh J, Cosgrove J, Sherkati S et al. (2024). Structural style and timing OF NW-SE trending zagros folds IN SW Iran: interaction with north-south trending arabian folds and implications for petroleum geology. Journal of Petroleum Geology 47 (1): 3–73. https://doi.org/10.1111/jpg.12850

Vernant P, Nilforoushan F, Haztfeld D, Abassi M, Vigny C et al. (2004). Present-day crustal deformation and plate kinematics in Middle East constrained by GPS measurement in Iran and northern Oman. *Geophysical Journal International* 157: 381–398. https://doi.org/10.1111/j.1365-246X.2004.02222.x

Wallis SR (1995). Vorticity analysis and recognition of ductile extension in the Sanbagawa belt, SW Japan. Journal of Structural Geology 17: 1077–1093. https://doi.org/10.1016/0191-8141(95)00005-X

Wallis SR, Platt JP, Knott SD (1993). Recognition of syn-convergence extension in accretionary wedges with examples from the Calabrian arc and the eastern Alps. *American Journal of Science* 293: 463–495. https://doi.org/10.2475/ajs.293.5.463

Wu W, Liu J, Zhang L, Qi Y, Ling C (2017). Characterizing a middle to upper crustal shear zone: microstructures, quartz c-axis fabrics, deformation temperatures and flow vorticity analysis of the northern Ailao Shan-Red River shear zone. Journal of Asian Earth Sciences 139: 95–114. https://doi.org/10.1016/j.jseaes.2016.12.026

Wu Y, Zhang J, Zhang B, Mao X, Lu Z et al. (2023). Early Paleozoic oblique convergence from subduction to collision: Insights from timing and structural style of the transpressional dextral shear zone in the Qilian orogen, northern Tibet of China. GSA Bulletin 136 (5-6): 1889–1915. https://doi.org/10.1130/B36947.1

Xypolias P (2010). Vorticity analysis in shear zones: a review of methods and applications. Journal of Structural Geology 32 (12): 2072–2092. https://doi.org/10.1016/j.jsg.2010.08.009

Xypolias P, Spanos D, Chatzaras V, Kokkalas S, Koukouvelas I (2010). Vorticity of flow in ductile thrust zones: examples from the Attico-Cycladic Massif (Internal Hellenides, Greece). In: Law, R, Butler, R, Holdsworth, B, Krabbendam, M, Strachan, R. (eds) Continental Tectonics and Mountain Building. Geological Society, London, Special Publications 335: 687–714. https://doi.org/10.1144/SP335.28

Zonenshain LP, Pichon X (1986). Deep Basins of the Black Sea and Caspian Sea as Remnants of Mesozoic Back-Arc Basins. Tectonophysics 123: 181–211. https://doi.org/10.1016/0040-1951(86)90197-6